Walking entrains unique oscillations in performance on a visual detection task

Matthew J. Davidson[1*], Frans A.J. Verstraten[1], & David Alais[1]

Affiliations:

1) School of Psychology, The University of Sydney, Australia

* Corresponding author (matthew.davidson@sydney.edu.au)

Abstract

Walking is among our most frequent and natural of voluntary behaviours, yet the consequences of locomotion upon perceptual and cognitive function remain largely unknown. Recent work has highlighted that although walking feels smooth and continuous, critical phases exist within each step-cycle for the successful coordination of perceptual and motor function. Here, we tested whether these phasic demands impact upon visual perception, by assessing performance in a visual detection task during natural unencumbered walking. We finely sampled visual performance over the stride cycle as participants walked along a smooth linear path at a comfortable speed in a wireless virtual reality environment. At the group-level, accuracy, reaction times, and response likelihood showed strong oscillations, modulating at approximately 2 cycles-per-stride (~2 Hz) with a marked phase of optimal performance aligned with the swing phase of each step. At the participant level, Bayesian inference of population prevalence revealed highly prevalent oscillations that clustered in two idiosyncratic frequency ranges (2 or 4 cycles per stride), with a strong phase alignment across participants.

Introduction

It is vital for our survival to correctly perceive and act within a dynamic environment. While the world is self-evidently dynamic, so too is the perceptual observer. In a typical day we may make over 150,000 saccades, 15,000 head-turns, and take several thousand steps (Carpenter, 1988, 2000; Hillnhütter, 2022). To test perceptual processes in contexts that are closer to which evolution has optimised them, we therefore need to take experiments out of darkened, static laboratories and into more complex, active situations. Here we examine the influence of the active observer during walking and test continuous visual performance, specifically focusing on the time-course of performance within the stride cycle. Despite the thousands of steps we take each day, the influence of locomotion upon perception is largely unexplored, and within-gait modulations have received no attention. Previously, the technical limitations of controlling an environment for active perception have been high, but here we use wireless and position-tracked virtual reality to probe visual detection performance continuously during locomotion. We find that walking entrains rhythmic changes to perceptual performance *within* each stride-cycle, despite the seemingly continuous and effortless nature of this everyday behaviour.

Studies examining the effects of walking and exercise on cognitive function have usually focused on changes in performance over an extended period of activity, rather than effects occurring within the stride cycle. These studies have found that when various forms of light exercise and stationary conditions are compared, periods of moderate exercise can induce small increases in performance on cognitive tasks (reviewed in Chang et al., 2012), and in neuroplasticity (Lunghi & Sale, 2015). Others have focused on how the presence of a dual-task during walking affects gait parameters such as speed and variability (Al-Yahya et al., 2011). More recent reports have demonstrated that walking or light exercise can enhance visual processing relative to stationary conditions (Bullock et al., 2017; Cao & Händel, 2019; Chen et al., 2022a, 2022b; Dodwell et al., 2021; Garrett et al., 2021). These results echo earlier work in animal models which has demonstrated how locomotion elevates the response gain of early visual processing areas – potentially providing a mechanism for enhanced performance on visual processing tasks (Ayaz et al., 2013; Busse et al., 2017; Dipoppa et al., 2018; Niell & Stryker, 2010; Parker et al., 2020). Critically however, most of these studies have focussed on average performance *over* the exercise period, or immediately after exercise, and have not studied temporal changes *within* the stride cycle.

There are a variety of findings that suggest visual performance might vary over the stride cycle. Recent investigations have demonstrated that responses to visual information depend on the phase of human locomotion (Burkitt et al., 2020; Chiovetto & Giese, 2013; Matthis et al., 2017, 2018). Humans capitalise on the pendulum-like momentum of each step when planning subsequent footsteps (Matthis & Fajen, 2013), and visual information about

the upcoming terrain must be received within a critical window prior to heel-strike for smooth locomotion to occur (Matthis et al., 2017). In addition, eye-movements (Cao et al., 2020; MacNeilage, 2020; Matthis et al., 2018; Mulavara & Bloomberg, 2002) and the accuracy of visuomotor coordination (Davidson et al., 2023) also show a coupling to the phase of locomotion. Together, there are a range of dynamic demands that occur with each step, which may result in modulations of visual processing while we walk.

Here we introduce a new method that allows us to finely sample performance in a simple visual detection task while walking, to test for modulations over the time-course of the stride cycle. During natural unencumbered walking we found that average accuracy, reaction times, and the likelihood of manual responses on a visual detection task all oscillated within the stride cycle in primarily two frequency bands (~2 and 4 Hz). These new findings show that the continuous demands of walking impose rhythmic changes on both sensory processing and manual responding with every step. In doing so, we also validate our new fine-sampling approach that will enable further investigation of stride-cycle modulations of perception and performance.

Results

We examined performance on a simple visual detection task during natural walking within a wireless virtual reality environment. Participants responded as quickly and accurately as possible to brief targets appearing within a circular annulus that drifted slowly and randomly around the screen (**Figure 1**). Below, we first compare average performance between walking and stationary conditions, before turning to our main focus, which was whether performance would modulate relative to the phase of the stride cycle.

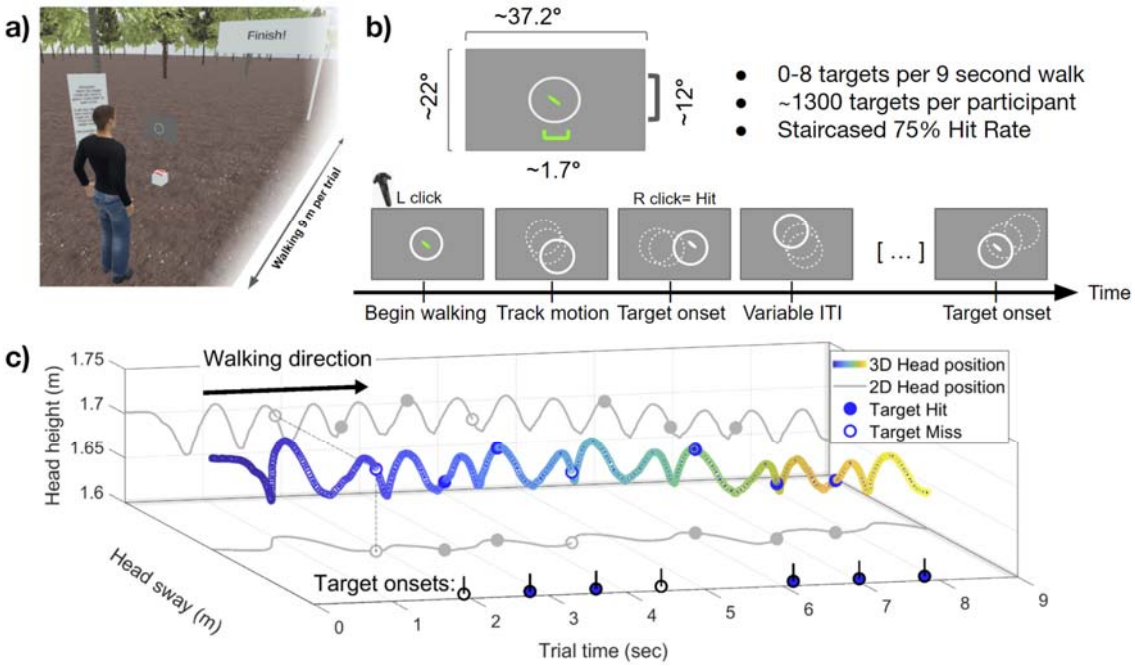

***Figure 1**. Environment and trial structure. **a)** Third-person view of the virtual environment. Participants were positioned behind a virtual grey screen displaying the target stimulus. During the trial, the screen progressed with smooth linear locomotion at a constant velocity, in line with a small walking guide (3-Dimensional animated game object). The avatar shown is for illustrative purposes only and was not present during the experiment. **b)** The visual detection task required participants to monitor a drifting circular annulus. Small target ellipses (1.7 d.v.a, 20 ms duration) appeared with a variable ITI, responses were provided via right trigger click. **c)** Example data from a single walking trial. Three-dimensional head position is recorded at 90 Hz (shown in blue). Walking produces a stereotyped sinusoidal pattern of head motion on the vertical axis (head-height, 2D projection on back-wall shown in grey). Peaks and troughs in head height correspond to the swing and stance phases of each step, respectively (see Methods). Our primary interest was whether the timing of target onset relative to stride-cycle phase would modulate task performance.*

Walking increases the threshold for visual target detection

Throughout the experiment, a continuous adaptive staircase procedure was implemented which manipulated target contrast to maintain participant accuracy at approximately 75%. Confirming this, average accuracy was close to 75% and not significantly different between stationary (M = 0.74, SD = .03) and walking conditions (M = 0.75, SD = .03, $t(35) = -0.32$, $p = .75$). The stationary condition, however, was clearly easier for participants because the staircase settled at a lower average target contrast (M = -7.12 dB; SD = 0.24) than in the walking condition (M = -6.87, SD = 0.50; $t(35) = 3.72$, $p < .001$, d

= .62).

While titrating contrast to maintain overall accuracy at 75%, target contrast on individual trials was presented at ± 3 intensity levels centred on the estimate required for 75% performance, to allow psychometric functions to be fitted over 7 contrast levels. Psychometric fits to participant accuracy revealed that the accuracy difference between standing and walking conditions was driven by a change in threshold ($t(35) = -5.06$, $p < .001$, $d = -.67$). There was no change in the slope parameter between stationary and walking conditions ($p = .32$). Interestingly, reaction times to targets were faster on average in walking compared to stationary conditions ($t(35) = 2.47$, $p = .018$, $d = .41$). There was also an inverse relationship between reaction times and accuracy across intensity levels, indicating participants were more accurate when responding quickly. A 2 x 7 repeated measures ANOVA (walking condition x contrast level) indicated main effects of condition ($F(1,35) = 6.12$, $p = .018$, $\eta_p^2 = .15$) and contrast ($F(6,210) = 118.60$, $p < .001$, $\eta_p^2 = 0.77$) with no interaction ($p = .06$). **Figure 2** displays a summary of this data.

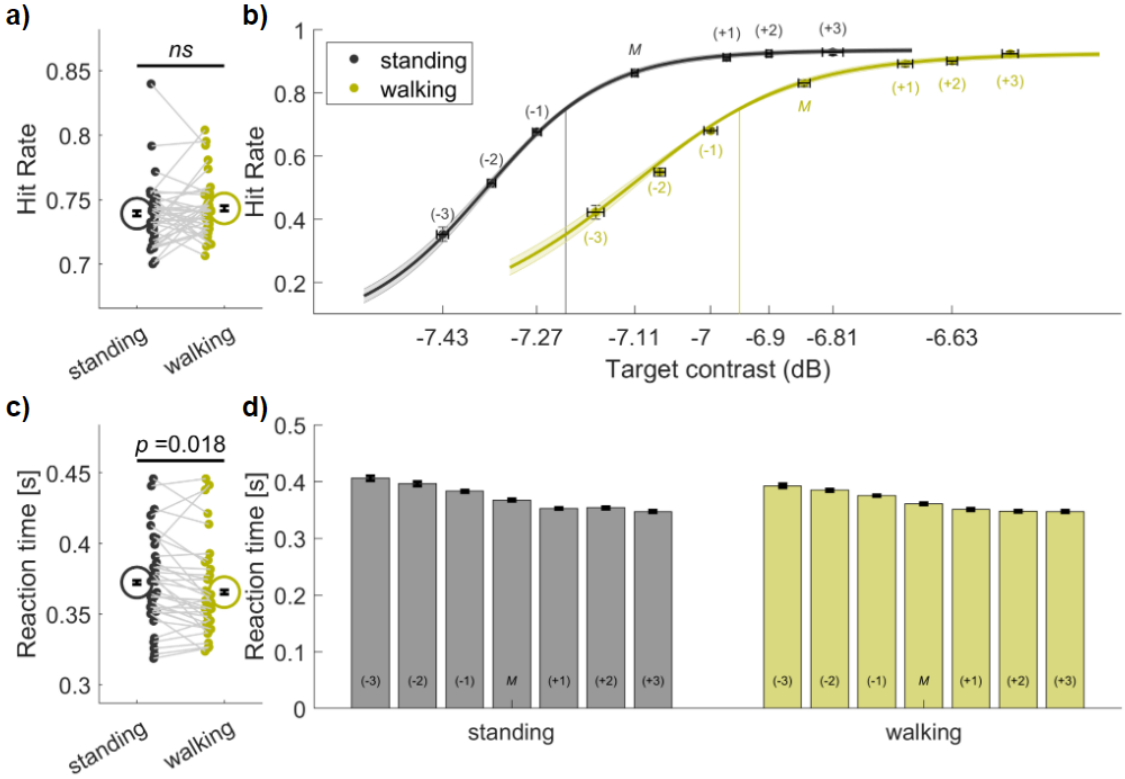

Figure 2. *Comparison of detection, hit rate and reaction time when standing and walking.* ***a)*** *On average, no difference in accuracy between conditions as a result of the adaptive staircase procedure. Black colours indicate standing, yellow indicate walking. Grey lines link participant data, circles display the group mean and error bars display ±1 SEM corrected for within participant comparisons (Cousineau, 2005).* ***b)*** *Psychometric fits to hit-rate data for each condition. The staircase mean for each condition is indicated M, contrast steps (see Methods) are indicated numerically in the range of -3 to +3. Vertical error bars represent ±1*

SEM for hit-rate, horizontal error bars represent ±1 SEM for adaptive target contrast. ***c)*** *Reaction times for correct detection decreased when walking, compared to standing (colours as in b), and* ***d)*** *reaction times decreased as accuracy improved over the psychometric function.*

Performance oscillates within the stride-cycle

We next compiled the 100s of detection data points (*M* = 885.52, *SD* = 63.33 per subject) into a single stride cycle in order to test for temporal modulations of visual performance. For this analysis, we first epoched all walking trials into stride cycles (two sequential steps), by running a peak-detection algorithm on the head-height time-series recorded on each trial. This analysis revealed that step- and stride-duration varied across participants (step duration M = 0.59 sec, SD = 0.034; stride M = 1.18, SD = .069). Supplementary Figure 4 visualises an example participant and the group-level stride-cycle variability. As is common in gait-based research, we next resampled all strides to 1-100% stride completion, to facilitate within- and across-participant averaging for our main effect of interest – whether the relative phase of an individual's stride-cycle would modulate visual detection performance. Target onsets, which were presented at random times, could thus be allocated to a position relative to the stride within which it occurred (from 1-100%; see **Figure 3A-C** for key stages of this workflow). In effect, the 100s of data points are pooled into a single, densely sampled stride that can be resolved into fine time bins (e.g. 2.5% bin width **Figure 3**) and reliably analysed for temporal modulations. **Figure 3C** plots target density over the stride cycle and validates our random-probing and stride epoching procedure as the distribution is flat with ~18 (*M = 17.84, SD = 1.2)* targets falling in each bin.

The stride cycle analysis revealed clear oscillations in performance on the visual detection task. **Figures 3D-F** display the group average results (*n* = 36) when binned into 40 linearly spaced, non-overlapping bins. The solid curves display the best-fitting first-order Fourier model (see Equation 1). **Figure 3G** shows the goodness-of-fit (R^2) for all Fourier frequencies in the range from .2 to 10 cycles per stride (cps; in steps of .2 cps). For accuracy, the best-fit to performance over the stride cycle was at 1.93 cps (R^2 = .48), and group-level fits were above the 95th percentile of the R^2 distribution obtained by permutation (*n* = 1000) for the range 1.80 – 2.20 cps. For reaction times, the best-fitting oscillation was at 2.02 cps (and was significant over the range 1.60 – 2.40 cps), and for manual response likelihood, the best-fitting oscillation was at 1.90 cps (significant from 1.60 – 2.20 cps).

We performed several control analyses to confirm these oscillations were driven by the stride-cycle. We first examined performance with respect to trial-onset, using clock-time (rather than stride-cycle) as our reference for entrainment. For this analysis, we averaged each of the behavioural variables considered based on consecutive 1 second epochs in both the walking and standing data. Although these 1 second epochs are a rough approximation of average stride-duration in our sample, the fit-strength of Fourier models was far weaker

than that based on stride-alignment (Supplementary Figure 6). As expected, equivalent results were found in the same analysis applied to standing trials (Supplementary Figure 7). These results provide complementary evidence that stride phase aligns the modulations in behavioural performance we report, rather than an alternative explanation based on trial-time.

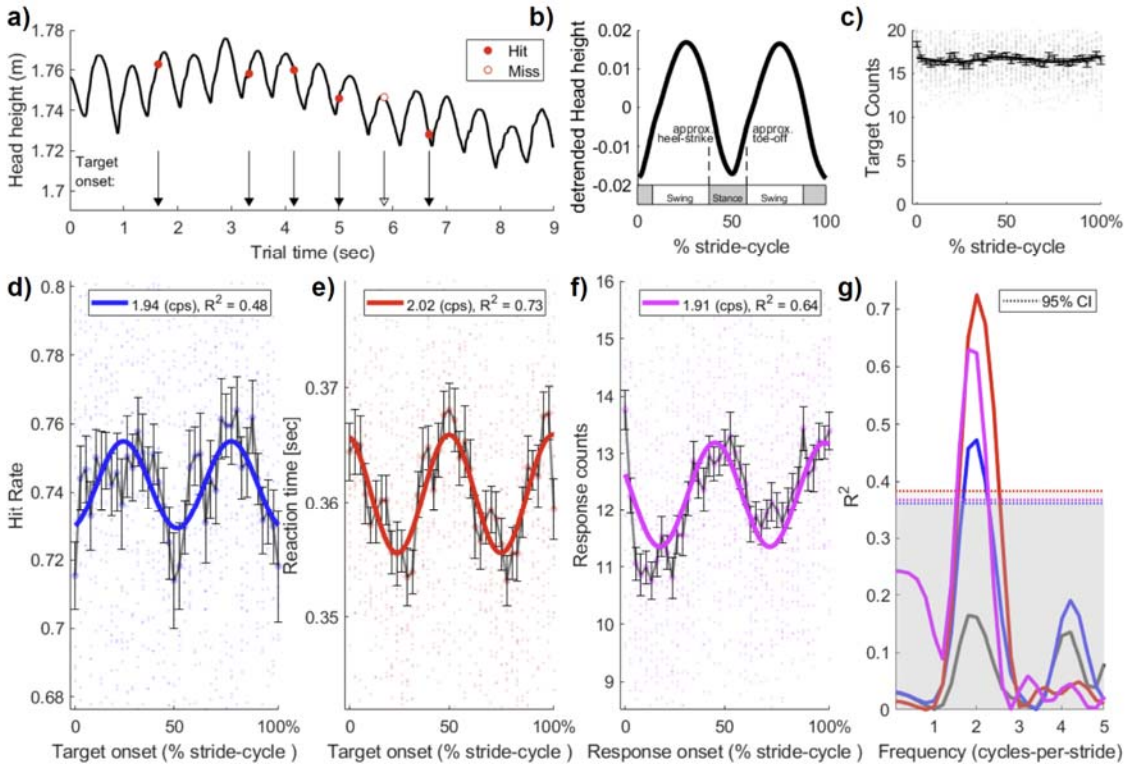

Figure 3. *Performance oscillates over the stride-cycle.* ***a)*** *An example trial from one participant, displaying the position-tracked vertical head-height over time whose peaks and troughs are used to define the steps. Target onsets are displayed with black arrows, and red markers indicate the behavioural outcome on the task (Hit, Miss) with red markers.* ***b)*** *To allow pooling of data over participants each stride (two steps) was resampled to a normalised range of 1–100%. Approximate swing and stance phases of the stride cycle are displayed above the x-axis.* ***c)*** *Target presentation density was approximately uniform over the stride cycle, validating the random-probing and stride-epoching procedure.* ***d-f)*** *Group level data (N=36) show clear oscillations over the stride cycle for detection accuracy (hit-rate), reaction time, and the likelihood of manual responses. The best-fitting first-order Fourier model is shown in each figure and approximated 2 cycles per stride (i.e. the step rate).* ***g)*** *Permutation testing of the best-fitting Fourier models. The observed data in c-f were fitted with a single-component Fourier model at all frequencies between .2 and 10 cycles per stride (in steps of .2) and goodness-of-fit (R^2) was calculated. The prominent peaks at approximately 2 cps show that the best fits, whether for accuracy (blue), reaction times (red), or responses (magenta) occur at approximately 2 steps per stride far exceed the 95% permutation confidence interval calculated using the maximum test statistic across all frequencies per permutation (dotted lines and grey shading). These peaks did not co-occur with above-chance fluctuations in the likelihood of target presentation, which is shown by the grey line.*

Population prevalence of stride-cycle oscillations

In addition to the group-level test of oscillations in performance, we tested the population prevalence of oscillations within our sample. Qualitative observations of our data showed some participant-level Fourier fits occurred outside the group-level best fit of

approximately 2 cps. We therefore formally quantified the prevalence of significant oscillations in the .2– 10 cps range per individual participant.

Consistent with the group-level results, we found oscillations at approximately 2 cps were the most prevalent in the sample. For example, for oscillations in accuracy, 12 of 36 participants had strong fits at approximately 2 cps that exceeded the 95% confidence interval of their shuffled data, rejecting the null at the participant level null-hypothesis significance test (NHST). Similar results were found for reaction time (*n* = 13/36 NHST at 1.5 – 2.5 cps), and response likelihood (*n* = 17/36 at 1.5 – 2.5 cps). Notably, a large proportion of our sample exhibited significant oscillations at higher frequencies, particularly at approximately 4 cps (accuracy *n* = 13/36; reaction times *n* = 14/36; responses *n* = 9/36 at 3.5 –4.5 cps). Subsequent analysis indicated these individual level oscillations, though idiosyncratic, were highly reliable. Few participants displayed significant oscillations in multiple frequency bands on any one measure (accuracy *n* = 4; reaction times *n* = 2, responses *n* = 3). Most displayed the same individual oscillation across all three measures, with very few having different oscillations across performance measures (*n* = 3/36). **Figure 4A-F** displays a summary of this data, showing the strength of individual participant Fourier fits at each frequency in cycles-per-stride. A small subset of participants demonstrated no significant oscillation on each measure (accuracy *n* = 6, reaction times, *n* = 3; responses *n* = 3 see **Figure 4G-I**).

We proceeded by formally quantifying the population prevalence of these oscillations using Bayesian inference. Bayesian inference of population prevalence provides an estimate of an effect's within-participant replication probability, and is particularly useful when examining effects which may be heterogeneous (Ince et al., 2021, 2022). This method returns the maximum *a posteriori* (MAP) estimate of the population prevalence, and a 95% confidence interval within which the MAP resides. For example, the prevalence estimate for oscillations in accuracy at 2 cps is .32 (MAP), with a 95% HDPI between [.18, .49], indicating a 95% probability that the population prevalence of oscillations in accuracy at 2 cps exceeds .18. Similar results were found for reaction time (2 cps, MAP = 0.30, [0.16, 0.47]) and response likelihood (2 cps, MAP = 0.41, [.26, .58]). Given the idiosyncratic yet reliable presence of oscillations, the Bayesian estimate for *any* oscillations in each of our measures over the range .2– 10 cps was very high. For accuracy 29/36 participants demonstrated oscillations in the .2–10 cps range (MAP = 0.82, [.68, .93]), 33/36 participants displayed oscillations in reaction times (MAP = 0.91 [0.79, .98]), and 32/36 for oscillations in response likelihood (MAP = 0.88, [.75, .96]). **Figure 4J-L** displays the prevalence estimates for oscillations at 2, 4, and any cycles per stride, for each of our dependent measures.

We performed additional exploratory analyses to investigate whether these idiosyncratic frequencies correlated with raw stride-cycle duration. One possibility is that these oscillations are not determined by stride-cycle, but a more general oscillator such as clock-time, which when resampled over different stride-lengths could result in the variability

in peak cps we observe. As a toy example, a single oscillator at 4 Hz could be captured as a 2 cps or 4 cps oscillation, within individuals with a 500 ms vs 1000 ms stride-length, respectively. In our data, we observed no relationship between the across-participant stride length and the strength of 2 cps fits, strength of 4 cps fits, nor the frequency of maximum fit strength, for any of our dependent variables (Supplementary Figure 5). Thus, it is the phase of the stride-cycle that matters, not the duration of each step. When aligned by phase, clear group effects emerge. Together, these results indicate that significant oscillations in visual detection task performance occur in over 80% of our sample, with stable idiosyncratic frequencies in performance per participant.

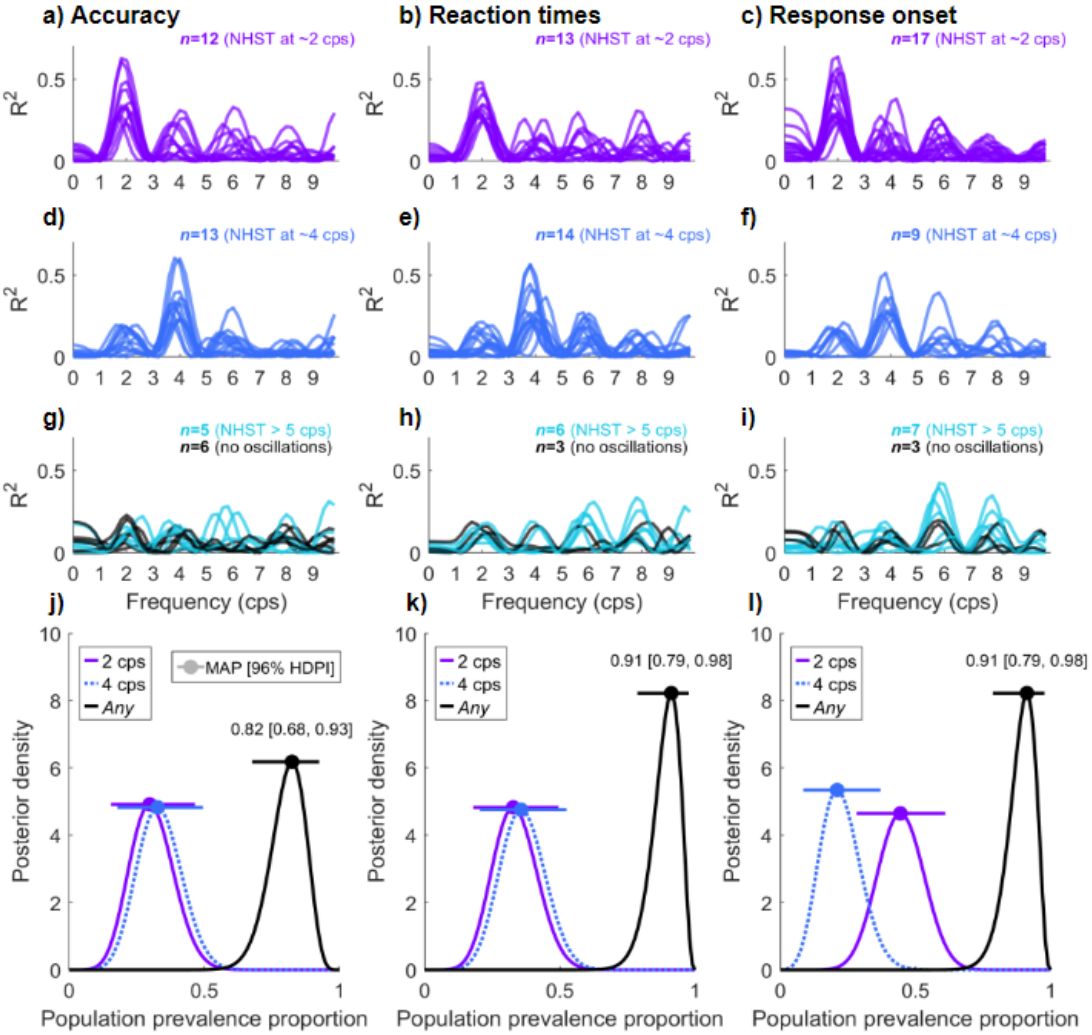

Figure 4*. Population prevalence of performance oscillations over the stride-cycle.* ***a)*** *Subset of participants displaying significant oscillations in accuracy performance between 1.5 and 2.5 cycles per stride (cps). Each line is the Fourier fit strength to participant-level data between .2 and 10 cps (in steps of .2). The strength of the participant-level Fourier fit was compared to the 95% Confidence Interval of permuted data, per participant (see Methods). For accuracy, 12/36 participants demonstrated significant oscillations at approximately 2 cps.* ***b-c****) Display the same result for reaction time and response likelihood oscillations at 2 cps, respectively.* ***d-f)*** *Independent subsets of participants with significant oscillations between 3.5 and 4.5 cps).* ***g-i)*** *Remaining participants with significant oscillations either above 5 cps (n = 5, 6, and 7 out of 36 for accuracy, reaction time, and responses, respectively), shown in magenta. Overlaid in dark grey are the fits for participants with no significant oscillation at any frequency (n=6, 3, 3 for accuracy, reaction time, and responses, respectively).* ***j-l)*** *Bayesian estimates of population prevalence for oscillations at 2 cps (purple), 4 cps (blue-broken lines), or any frequency in the range .2 – 10 cps (black). Circular markers display the maximum a posteriori estimate of prevalence (MAP), and error bars display the 95% HDPI (see Methods).*

Oscillations in performance are phase-aligned across participants

Our previous analyses demonstrated that oscillations in visual detection performance

are highly prevalent within our sample and occur at stable idiosyncratic frequencies per participant. We next inspected whether the phase of these oscillations would also be consistent across participants. For this analysis, we included only the subset of participants that displayed significant oscillations when compared to their shuffled likelihood, and below focus on those participants with oscillations in the 1.5 – 2.5 cps range (accuracy data n = 12, reaction times n = 13, response likelihood n = 17). The best-fitting Fourier model was calculated per participant and the phase retained for subsequent tests of non-uniformity. **Figure 5** displays the phase results and shows the individual data are tightly clustered in phase. Optimal accuracy (**Figure 5A**) and reaction time (**C**) occur in the approximate swing phase of the stride cycle, while response likelihood (**E**) entrains to the time of heel strike. Rayleigh's test confirmed that two of these phase distributions were non-uniform (accuracy; Z =3.62, p = .023; reaction time; Z = 3.59, p = .024; response Z = 4.73, p = .007).

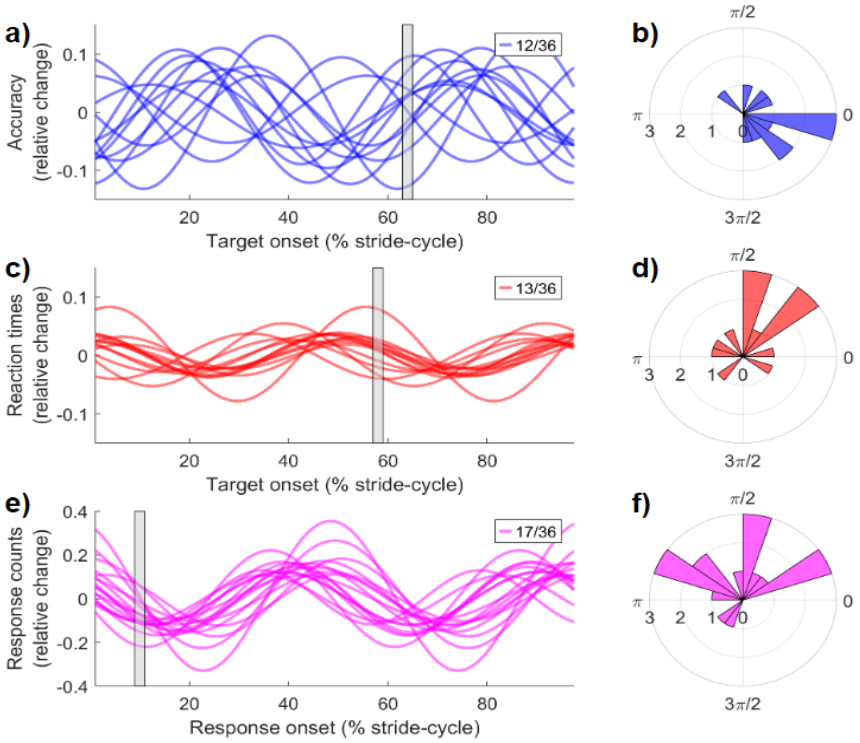

***Figure 5. Participant-level oscillations in performance are clustered in phase**. **a)** For participants with significant oscillations in accuracy at approximately 2 cycles per stride (n = 12), the Fourier series model at 2 cycles per stride is displayed. To ease interpretation of differences in phase, participant-level data is expressed in relative change from their mean ((X-Mean) / Mean). The vertical grey shaded region notes the time at which the phase distribution in b corresponds to. **b)** displays the polar plot of phase across participants. **c-d**) Reaction time data (n = 13). **e-f)** Response onset likelihood (n = 17).*

Discussion

We investigated whether the natural phases of human locomotion alter performance on a simultaneous visual detection task. Participants walked along a path in a wireless position-tracked virtual reality environment and responded as quickly as possible to brief visual targets presented at random intervals as they walked. An offline analysis of head-height data was used to define the start and end of each stride cycle, and to determine the timing of the target relative to stride onset. Pooling over many trials and dividing the data into fine time bins, we confirmed that targets occurred uniformly across the stride cycle. However, analysing accuracy, reaction time, and manual response likelihood revealed clear oscillations in all three performance measures that were systematically linked to the phase of locomotion. Further analyses of individual participants confirmed that these group level performance oscillations were present in a large proportion of our sample, predominantly at

either 2 or 4 cycles per stride (cps). While the frequency of 2 or 4 cps was idiosyncratic, there was a strong consistency within participants so that the same frequency was seen for a given participant across the three performance measures.

Together, these results reveal for the first-time systematic modulations of visual performance within the stride cycle. This work also validates our new approach as a viable method that will enable further research into stride-cycle modulations of perception and performance in vision and other sensory modalities.

What might underlie these oscillations in performance during locomotion? It is important to note that oscillations are a ubiquitous feature in neuroscience, in both brain and behaviour (Fiebelkorn & Kastner, 2019). Prior work has established that performance on a visual detection task waxes and wanes over time (see (Tosato et al., 2022; VanRullen, 2016) for reviews). These behavioural oscillations are in the theta or low alpha range (4 –10 Hz), and have been variously linked to the reallocation of attention (Landau & Fries, 2012; VanRullen, 2018; VanRullen et al., 2007) to perceptual sampling (VanRullen, 2015), or to decisional processes (Zhang et al., 2019). Often in these studies of behavioural oscillations, a salient transient stimulus is used to ‘reset’ the phase of ongoing oscillations (Davidson et al., 2018; Romei et al., 2012) so that they can be probed from a known and repeatable temporal reference point. For example, this approach has been used to reveal oscillations in perceptual sensitivity in both vision and audition (Ho et al., 2017; Zhang et al., 2019), and counterphase oscillations that have been linked to the reallocation of attention (Fiebelkorn & Kastner, 2019; Fiebelkorn et al., 2013; Landau et al., 2015).

Behavioural oscillations can also be revealed by using an action at the start of the presentation period to reset the phase of neural oscillations. Actions as simple as reaching or making a button press are sufficient to provide a time-zero point from which underlying oscillations can be probed over time (Benedetto et al., 2016; Tomassini et al., 2015, 2017; Wutz et al., 2016). Our work, though, is the first to identify oscillations in performance that are synchronised to the rhythmic action of locomotion. On average our participant group exhibited best-fitting Fourier frequencies which spanned the range 1.93 – 2.02 cycles per stride (**Figure 3D-F**). This raises the possibility that the act of taking a step resets the phase of neural oscillations and creates a repeatable reference point that causes an underlying oscillation to be revealed at approximately the step-rate. It remains to be seen whether the oscillations we have described co-occur with slower endogenous brain rhythms, as has been the case for previous work investigating the fast-scale oscillations at higher rates in performance linked to attention and perceptual sampling (Fiebelkorn et al., 2018). Similarly, reaching behaviour has been shown to reset the phase of endogenous oscillations (Tomassini et al. 2017; Tomassini et al. 2020; Benedetto et al. 2020) and the ballistic movements generating locomotion may reset or entrain neural oscillations relevant to

behavioural performance (Schroeder et al. 2010).

One interpretation of the oscillations observed in perception and attention is that they arise naturally as a kind of reverberation frequency. On this view the period length reflects the time taken for signals to feed forward to higher-level areas and then feed back to sensory levels. A similar pattern could arise in locomotion at a lower frequency governed by the step rate. Locomotion obviously involves feedforward motor signals, but the control of locomotion is not possible without neural and mechanical feedback (Dickinson et al., 2000; Lacquaniti et al., 1999). There are also numerous findings in rodents showing that locomotion elevates sensory cortical response gain generally and visual cortical activity specifically (Ayaz et al., 2013; Bullock et al., 2017; Dipoppa et al., 2018; Keller et al., 2012; Niell & Stryker, 2010; Parker et al., 2020; Polack et al., 2013; Saleem et al., 2013). It is not known yet whether these condition-average elevations interact with the phases of the stride cycle, but this established link between locomotion and visual cortical activity raises a testable and more specific proposition that the stride cycle may modulate activity in visual cortex and thus produce oscillations in visual performance entrained to each step.

Also relevant to the present work are recent studies investigating brain-body coupling in the context of perception and motor commands. The rhythmic influences of the cardio-respiratory system, for example, are increasingly recognised to contribute to variability in perceptual task performance (Allen et al., 2022; Azzalini et al., 2019; Critchley & Harrison, 2013; Heck, McAfee, Liu, Babajani-Feremi, Rezaie, Freeman, Wheless, Papanicolaou, Ruszinkó, & Kozma, 2016; Heck, McAfee, Liu, Babajani-Feremi, Rezaie, Freeman, Wheless, Papanicolaou, Ruszinkó, Sokolov, et al., 2016; Klimesch, 2018; Kluger et al., 2021; Kluger & Gross, 2021; Park et al., 2014; Varga & Heck, 2017). Our findings extend this line of work by showing how steady-state locomotion also rhythmically alters sensory performance, and that these effects are highly prevalent and idiosyncratic. Notably, heart-rate (Kirby et al., 1989; Niizeki et al., 1993, 1996; Niizeki & Saitoh, 2014), and respiration (Bernasconi & Kohl, 1993; Bramble & Carrier, 1983; Lee & Banzett, 1997) also show coupling to walking behaviour – leaving open the possibility that the oscillations we describe may also be synchronised with the cardio-respiratory, or other bodily systems (Klimesch, 2018). One intriguing possibility is that the variations in idiosyncratic peak frequency we report are not coupled to stride-cycle duration (cf. Supplementary Figure 4) but cardiorespiratory exertion. Future studies can individually calibrate walking speeds, as well as experimentally decouple the cardio-respiratory cycle from the stride-cycle (such as while carrying a backpack, or during inclined walking), to investigate this potential confound.

Similarly, recent work has identified that the timing of blinks and saccades also entrain to the rhythm of footfall (Cao et al. 2020), and that faster perceptual fluctuations may

be time-locked to saccade offset (Hogendoorn 2016). In our data the occurrence of saccades and blinks were relatively sparse owing to the smooth-pursuit nature of our task, yet future work could quantify the relative contribution of saccades to these oscillations using tasks that evoke large eye movements – for example, by presenting targets that vary unpredictably in peripheral eccentricity to the left or right of fixation.

The relative timing of the modulations in visual task performance we report are also noteworthy for other reasons. Previous work has indicated how the subjectively smooth nature of walking is nevertheless supported by phasic periods of enhanced sensory demand. In particular, after toe-off in the early phase of the step-cycle, and prior to heel-strike, the predictability of head movements are at their lowest (MacNeilage & Glasauer, 2017), leading to an increase in the weighting of vestibular signals to maintain balance and posture (Bent et al., 2004; Dakin et al., 2013). Indeed, it is well established that the evolution of locomotion required the widespread coordination of a host of bodily systems (Drew & Marigold, 2015; Grillner & El Manira, 2020). In animal models, a key result from this research is that although walking may appear smooth and continuous, there are phasic periods within each step-cycle that ballistically determine an ongoing step trajectory (reviewed in (Drew & Marigold, 2015; Grillner & El Manira, 2020).

In summary, while an increasing body of work has compared stationary conditions to light exercise, or continuous walking (Bullock et al., 2017; Cao & Händel, 2019; Chen et al., 2022a, 2022b; Cortney Bradford et al., 2019; Garrett et al., 2021), we have demonstrated that reliable measurements can be made within the stride cycle. In the current paper, this has revealed clear changes in visual performance linked to the phase of the stride cycle. These new findings open many research possibilities concerning, for example, how and where attention is allocated over the stride cycle, whether visual modulations occur uniformly over the visual field, and whether performance on auditory or tactile tasks will also modulate with locomotion.

Methods & Materials

Participants

We recruited 45 healthy volunteers, 7 of whom were excluded for incomplete data collection that either resulted from wireless signal drop-out or hardware malfunction. One more was excluded on the basis of eye-movement data (detailed below), and another for an error in eye-movement calibration. The remaining 36 volunteers included 22 females (Mean age = 19.6, *SD* = 2.6), with normal or corrected to normal vision. This study was approved by the University of Sydney Human Research Ethics Committee (HREC 2021/048), and all

participants were recruited from the University of Sydney undergraduate psychology cohort and received either course credit or 20 AUD per hour of their time.

Apparatus and virtual environment

The virtual environment was built in Unity (version 2020.3.14f1) incorporating the SteamVR Plugin (ver 2.7.3; SDK 1.14.15), on a DELL XPS 8950, with a 12th Gen Intel Core i7-12700K 3.60 GHz processor, running Microsoft Windows 11. The virtual environment consisted of an open simulated woodland, sparsely populated with trees, and has been described in detail previously (Davidson et al., 2023). In brief, participants walked along a simulated 9.5 metre track wearing the HTC Vive Pro Eye with integrated head-mounted display (HMD), a wireless adapter kit (130-gram weight) and carried two wireless hand-held controllers. The HMD houses two 1440 x 1600-pixel (3.5” diagonal) AMOLED screens, with 110-degree field of view refreshed at 90 Hz. The HMD also integrates Tobii eye-tracking technology, from which we recorded gaze origin and gaze direction information using the native SRanipal SDK (v1.1.0.1). During the experiment, the three-dimensional coordinates of the HMD, gaze-origin, gaze-direction and hand-held controllers were sampled at 90 Hz resolution, using five HTC Base Stations (v 2.0). Participant responses were collected from the wireless controllers and for self-pacing the onset of each trial using a trigger button beneath the right index finger.

At the start of each trial, the starting position was indicated by a large red “X” on the ground. The red X positioned participants in line with a walking guide, which was a small cube (0.1 m on a side) at approximately waist height. The cube had a directional arrow on the superior face displaying the required direction of motion on walking trials, or a stop signal on stationary trials. Positioned above the walking guide on each trial was a rectangular screen (35 cm width, 20 cm height). The average Euclidean distance between our participants’ HMD and the virtual screen was 52 cm, resulting in an average screen size of 37.2° x 21.8° of visual angle The vertical centre of the screen was calibrated to 80% of the height of each participant’s standing HMD location. This height calibration standardised the approximate viewing angle to the screen across participants. In the centre of the screen was a circular annulus (11 cm diameter, 12.1°) which indicated the boundary of the region to monitor for potential target appearances. Within this circular region, targets were briefly flashed with a grayscale contrast that was titrated using an adaptive staircase to standardise performance across participants to approximately 75% (see ***Staircase procedure*** below). The screen colour was uniform grey (RGB 0.4, 0.4 0.4), and target shape was a small ellipse, 1.5 cm in length on its long axis (subtending 1.66°), tilted at ± 45**°** from vertical.

Procedure and Task Stimuli

Upon arrival, the participants read over the information sheet, became familiar with the testing area, and had the chance to ask questions before providing informed consent. They were given a brief overview of the wireless virtual reality equipment, hand controllers, and battery pack before beginning the first practice block which was always the stationary condition.

Each experiment contained 10 experimental blocks, with 20 trials per block. Each trial was 9 seconds in duration, spent either standing still or walking the 9.5 metre distance at a steady speed, with the smooth duration and speed of travel set by the walking guide. On stationary trials, participants stood motionless for 9 seconds, while on walking trials the walking guide progressed at a smooth speed of 1.1 m/s. The order of the first two blocks was pre-set (stationary, walking), after which the remaining 8 blocks were randomised (two stationary and six walking blocks). Through pilot testing, we observed that accuracy quickly settled to approximately 75% in both conditions due to our adaptive staircase procedure, and consequently increased the trial count for the walking condition to enable detailed stride-cycle based analyses, which was our main focus of interest (see ***Performance relative to stride-cycle*** below).

Within each 9 second trial, we carefully spaced target presentation times to enable sequential responses per trial. A maximum of eight targets were presented within each trial, with a minimum inter-trial interval of 0.8 seconds. Each target was 20 ms in duration with a titrated contrast determined by adaptive staircase (see Staircase Procedure below). The spacing of targets was relative to predefined anchor points (e.g. target 1 at 1.1s, target 2 at 2.3 s …), with an additional jitter (± 0.5 seconds) to decrease the predictability of target onset within each trial (while ensuring the minimum ITI was satisfied). To further decrease the predictability of target onset times, each target had a 10% chance of being withheld from presentation, resulting in a range of actual target presentation counts per trial per participant (Min = 0, Max = 8, M = 6.99, SD = 0.07), as well as increased range of inter-trial intervals overall (M = 0.92 seconds, SD = 0.10s). This procedure resulted in an average of 507.66 stationary targets per participant (SD=68.87), and 884.13 walking targets per participant (SD=60.42). Importantly, this target presentation methodology resulted in an approximately uniform distribution of target onsets over the stride cycle (**Figure 3**).

During each trial, target location was also manipulated to increase engagement and attention on task. The circular annulus defining the boundary for target appearances slowly drifted within the confines of the background screen (speed range of 0.1 – 0.6 m /s). Targets could appear anywhere within this circular boundary, excluding regions that overlapped with the circular annulus. **Supplementary Figure 1** displays a summary of all target positions throughout the experiment. Supplementary Figure X displays the average timing of all target onsets throughout the experiment.

Staircase procedure

Our adaptive staircase was an implementation of the QUEST procedure (Watson & Pelli, 1983), programmed in C# for the Unity virtual environment. Target contrast was adjusted on a single-trial basis separately for stationary and walking blocks. For both staircases, we set the initial target contrast to 0.45 (the background screen was 0.4). We set the initial slope (β) parameter for QUEST at 3.5, standard deviation to 2, with a lapse rate of 0.01, and floor at 0.5. Both staircases had a resolution of .004, ranging in contrast from 0.4 to 1.

The staircase procedure began after the first three trials of the first practice block, which were omitted from further analysis. During these first three trials, target contrast was set at the suprathreshold starting parameter of 0.45 to familiarise participants with an easier version of the task. For the remainder of the experiment, we additionally manipulated target contrast by perturbing the QUEST staircase on a target-by-target basis. As the QUEST procedure quickly converged to a contrast value that approximated 75% accuracy, we selected each target contrast from one of seven positions within the 25th to 75th percentile of the prior probability density function. These positions were selected to enable psychometric fits to participant data, and spaced at percentiles [25, 32.25, 37.5, 50, 62.5, 68.75, 75]. For simplicity, we refer to these locations as [Q-3, Q-2, Q-1, Quest mean, Q+1, Q+2, Q+3] henceforth.

Psychometric fits

Using the dispersion of contrast intervals described above, we modelled psychometric fits to participant data using a cumulative normal distribution, implemented in the psignifit toolbox (Schütt et al., 2016). From each function, we retained the 50% threshold, fit width (difference between the 5th and 95th percentile of the data), and slope parameter. Figure 2 displays the average of participant fits during stationary and walking conditions.

Eye movement data

We collected eye movements using the SRanpal SDK and integrated Tobii eye-tracking technology. Eye movements were calibrated at the start of each experiment using a 4-point calibration procedure following the manufacturers settings. Additional calibration was performed after any change to the headset (such as after breaks, between blocks). We recorded 3D coordinates of eye position and gaze direction at each frame of all trials at 90 Hz resolution and performed the following preprocessing steps to identify and omit blinks from our analysis.

First, whole-trial time-series of the eye-position and gaze direction data were tested

for outliers. Blinks were identified using gaze direction data on the basis of data discontinuities that exceeded ± 0.8 m. Raw time-series data was then interpolated from -200 ms before to +200 ms after each blink, using a modified Akima piecewise cubic Hermite interpolation. Identical windows were interpolated for the gaze origin and gaze direction time-series on both axes. Overall, a low number of blinks were detected overall, with a low participant average per 9 second trial (M=1.12, SD= 1.08, range .035 – 4.05). Consequently, there was a very low incidence of blinks overlapping with target onset (within ± 200 ms; M = .07, SD=.13, range 0–.63). After interpolation, the vertical eye position data was linearly detrended to enable averaging across participants of different heights. Next, the cartesian coordinates of gaze direction at target onset were converted to polar coordinates, centred on the target's location. All target events that appeared when gaze location exceeded 12.1 degrees of visual angle from the target's position were excluded from further analysis. This procedure was in place to ensure that participants were gazing within the approximate region of the circular annulus when targets were presented. This procedure identified one participant for exclusion based on a large number of missed targets, but otherwise demonstrated that participants faithfully tracked the circular annulus with their gaze, as a low number of targets were rejected on average per participant (*M* = 57.47, SE= 30.2, approximately 4% of targets).

Gait extraction from head-position data

We estimated the phases of the stride cycle by applying a peak-detection algorithm to the time-series of head position data. As walking results in near sinusoidal changes in the vertical centre of mass over time, troughs on the vertical axis of head position correspond to when both feet are placed on the ground during the double support stance phase(Gard et al., 2004; Hirasaki et al., 1999; Moore et al., 2001; Pozzo et al., 1990). We epoched all individual steps based on these troughs, and normalised step-lengths for stride cycle analysis by resampling the time-series data to 100 points (1-100% cycle completion). We also visually inspected individual head-position time-series during pre-processing to identify trials for exclusion, based on wireless signal drop-out or poor performance of the peak-detection algorithm. Over all participants, an average of 1.1 trials (*SD* =1.3) were rejected in this manner (range 0 – 5)**.**

Performance relative to the stride-cycle

Our main analysis compared performance on the visual detection task relative to

position in the simultaneously occurring stride cycle. To accomplish this, all target onsets were allocated to the percentile (from 1-100 %) at which the target occurred in the simultaneous step (**Supplementary Figure 2**), or stride (**Figure 3**). For single-step analyses, we averaged performance within 20 linearly spaced bins (1-5%, 6-10% etc., with zero overlap). For the stride cycle, the same procedure was performed over 40 linearly spaced bins.

We analysed detection accuracy and reaction time relative to the point of target onset within each stride cycle, as well as response likelihood (the frequency of self-initiated responses to targets). For each dependent variable, we tested for a significant oscillation via a two-step procedure. At the group-level, we fit a sequence of Fourier series models within a forced frequency range, stepping from .2 to 10 cycles per stride, in .2 increments, using MATLAB's curve fitting toolbox and the equation:

$$f(t) = a0 + a1 \times cos(wt) + b1 \times sin(wt) = Acos(wt + \phi)$$

Where *w* is the periodicity (cycles per stride) *t* is time, *a1* and *b1* are cosine and sine coefficients and *a0* is a constant. The resulting sinusoidal fit has amplitude *A* and phase . The routine implements a non-linear least squares method that minimises the summed squares of the residuals over 400 iterations. For each forced fit at each frequency, we retained the goodness of fit (R^2) as our critical value. **Figure 3** visualises the goodness of fit for each Fourier series model on the observed group-level data, with clear peaks at approximately 2 and 4 cycles per stride. Next, we performed a non-parametric shuffling procedure to assess the likelihood of these fits occurring by chance. Specifically, for each participant we shuffled the data allocated to each percentile bin at random (without replacement), before repeating the group-level analysis and fitting procedure described above. This shuffling procedure was repeated 1000 times, and the distribution of R^2 values at each frequency from shuffled data served as the null-distribution for the strength of sinusoidal oscillations at chance - when the temporal order of the stride cycle had been destroyed via shuffling. We compared the observed R^2 value, to the upper 95% Confidence Interval (CI) of the null distribution across all frequencies and interpreted the presence of a significant oscillation when the observed R^2 value exceeded this critical value (effectively controlling for multiple comparisons).

We performed a series of additional analyses to further explore these oscillations in performance. We note that our main results of oscillations in performance also occur at the minimal width of 100 bins per step-cycle. **Supplementary Figure 2** also displays that the result is present in single-step cycle analyses, and that clear oscillations are present without any averaging (i.e. individual bins for targets at 1-100% of the stride cycle). We next examined whether mechanical artefacts may be contributing to these effects. Given the

decrease in detection accuracy around the time of footfall (during the loading phase of the stride cycle), one specific possibility is that the impact of footfall drives a mechanical distortion through the HMD. We hypothesised that if footfall was introducing a mechanical perturbation to the HMD and subsequent visual display, then the time-series of pupil origin should show an increase in variability at this same time. However, no increase in the variability of pupil origin was observed, indicating minimal displacement of the HMD during this phase of the stride cycle. Instead, we see clear evidence of an active compensation of gaze-direction to account for changes in head-position, as has been reported in other studies (MacNeilage, 2020; Mulavara & Bloomberg, 2002). **Supplementary Figure 3** displays this result. We also note that transient mechanical distortions cannot account for the higher frequency oscillations in a large portion of our sample (see **Figure 4**), or the existence of counterphase modulations in performance in a subset of participants (i.e. separated from the time of heel-strike (see **Figure 5**).

We also repeated our main analysis to test for oscillations in performance when aligning to trial-onset, using clock-time as the basis of our Fourier fits. This allowed us to test for oscillations in standing data, as well as to compare whether the goodness-of-fits obtained when testing cycles-per-stride exceeded those we could measure when testing cycles-per-Hz.

Participant-level analysis and Bayesian population prevalence

We additionally performed the same fitting procedure on individual participant data, to test for the presence of a significant oscillation between .2 and 10 cycles per stride, per participant. Performing participant level null-hypothesis significance testing (NHST) also enabled a test of Bayesian inference of population prevalence - a recently proposed alternative to the population average effect size (Ince et al., 2021). Bayesian inference of the population prevalence has several advantages compared to the group level binary result of a NHST (Ince et al., 2021, 2022), and is particularly powerful when investigating effects that may be heterogenous within a particular sample. After quantifying the proportion of participants that have a significant effect, this method estimates the population prevalence (within-participant replication probability) and quantifies the maximum a posteriori (MAP) estimate from this posterior distribution. Importantly, Bayesian prevalence provides both the most likely value of the population parameter, but also an explicit estimate of uncertainty within which the population prevalence resides. Here, following the recommendations of Ince et al., 2022 we report the MAP and the 95% highest posterior density intervals (HPDI). These intervals provide the range within which the specified population parameter resides with 95% probability.

From the individual-level fits we also compared the phase distributions of oscillations

across subjects and tested for phase clustering using Rayleigh's test of non-uniformity (Berens, 2009). **Figure 5** displays the individual level fits (when significant), and phase distributions for performance oscillations at 2 cycles per stride.

Data Analysis and Availability

All analyses were performed in MATLAB (ver 2022a) or JASP (0.16.3.0). Psychometric fits were performed using the Psignifit toolbox (Schütt et al., 2016). All raw data and analysis codes are available on the repository https://osf.io/8djtq/. We have implemented ColorBrewer (Harrower & Brewer, 2003) and Perceptually Uniform Colormaps (https://bids.github.io/colormap/) to aid in data visualisation. The 3D avatar was placed in the Unity environment for illustration purposes only and is available from www.passervr.com.

Code Availability

Analysis codes to reproduce the analyses are available in the public repository https://osf.io/8djtq/.

Author contributions

MJD and DA designed the research. MJD completed the research and wrote the manuscript. All authors revised the final manuscript.

Supplementary Materials

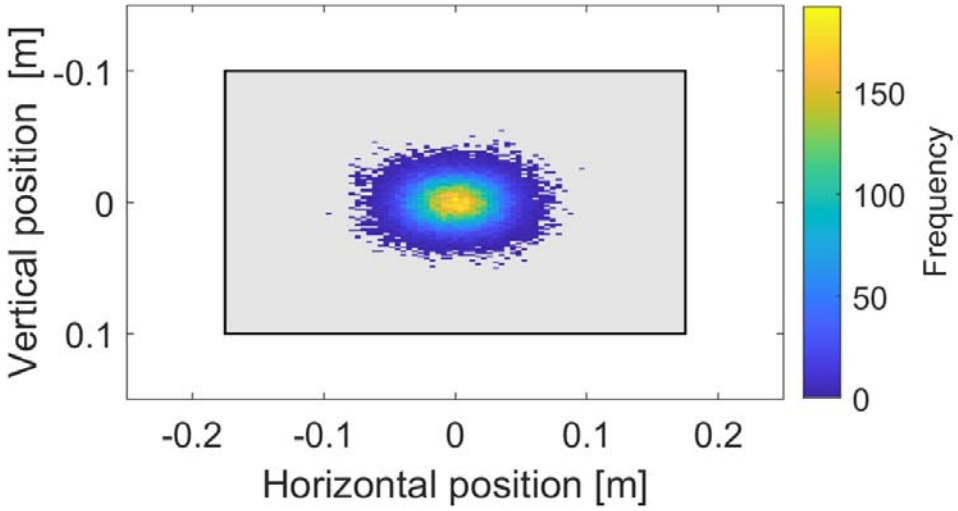

Supplementary Figure 1. *Distribution of all target locations throughout the experiment, relative to the centre of the virtual screen. Grey shaded region displays the approximate boundary of the virtual screen.*

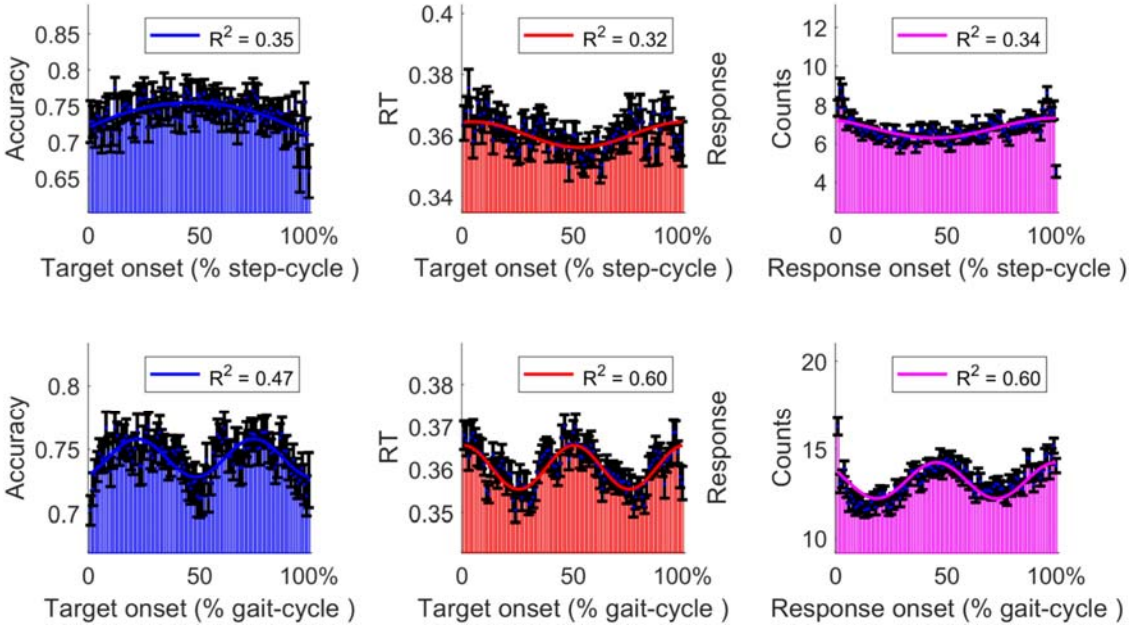

Supplementary Figure 2. *Oscillations in performance do not result from averaging within the linearly spaced bins in our stride-cycle analyses. Both rows reproduce the main results from Figure 3, omitting this procedure, with 100 data-points in a single-step analysis (top row), and 200 data points in the stride-cycle analysis (bottom row).*

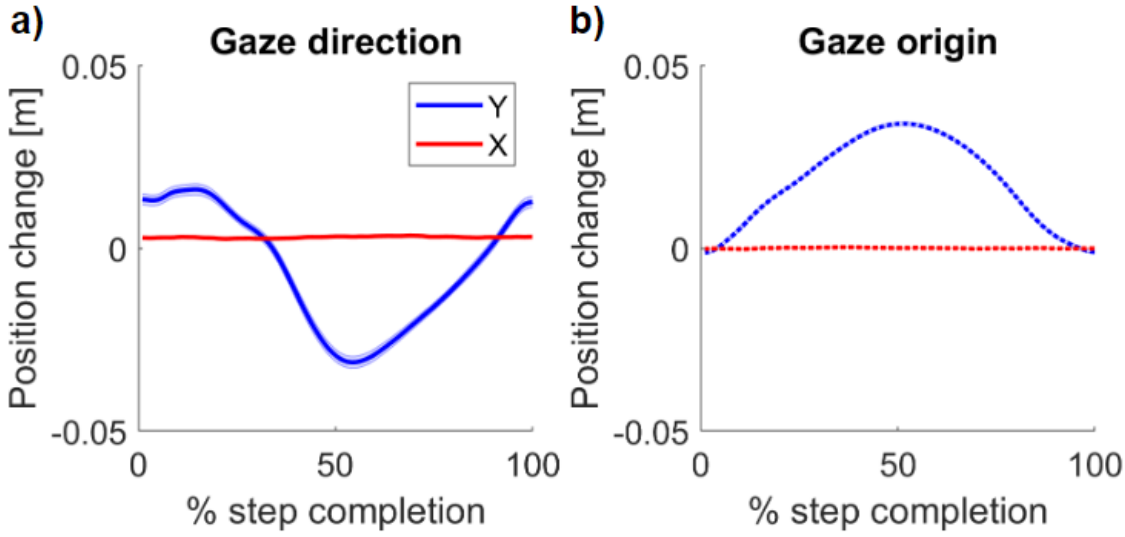

Supplementary Figure 3. *Gaze origin and gaze direction over the step-cycle.* ***a)*** *Average detrended gaze direction over a single-step cycle. A clear vertical translation occurs to compensate for changes in vertical head position.* ***b)*** *Average detrended change in gaze origin over the step-cycle. Like vertical head position, gaze-origin follows a smooth trajectory during the step-cycle, with no increase in variance around the time of footfall.*

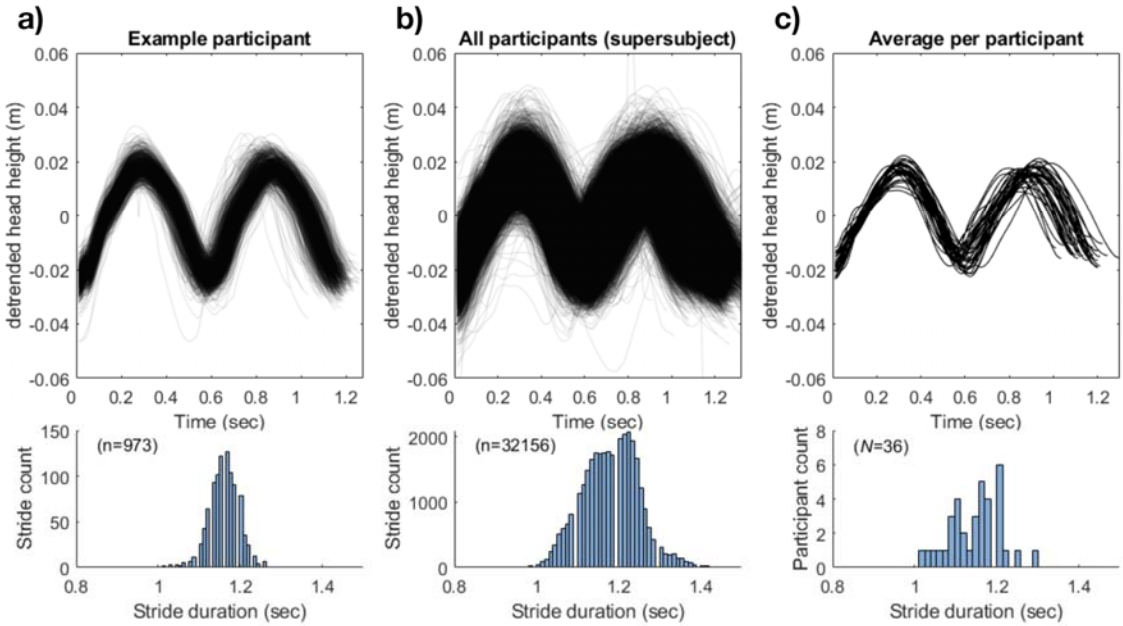

Supplementary Figure 4. *Example stride-cycle variability.* ***a)*** *The top panel displays the change in head-height (detrended) for all strides of a representative participant. The histogram of all stride durations (n=973) is displayed in the bottom panel.* ***b)*** *Top panel overlays all recorded strides, all participants, with the bottom panel showing the histogram of all stride durations.* ***c)*** *Top panel shows the average stride-cycle per participant, prior to resampling along the x-axis to 1-100% stride completion. The distribution of average participant stride durations is displayed in the bottom panel.*

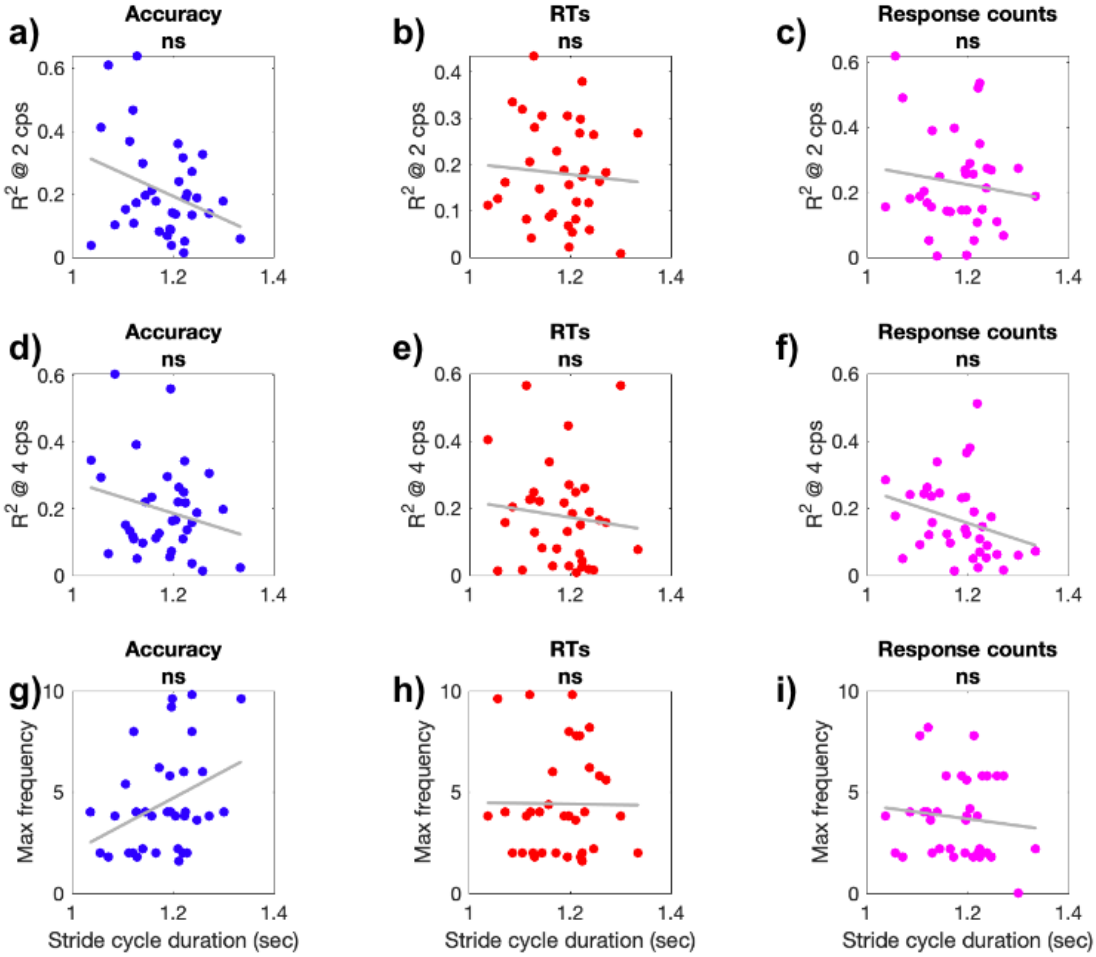

Supplementary Figure 5*. No correlation between participant stride-cycle duration and the idiosyncratic oscillations in perceptual performance.* ***a-c)*** *Display scatter plots (N=36) of the strength of Fourier fits at 2 cps (max between 1.8 and 2.2 cps) and average participant stride-cycle duration, for accuracy, reaction time, and response count data respectively.* ***d-f****) Display the relationship between the strength of Fourier fits at 4 cps (max between 3.8 and 4.2 cps) and stride-cycle duration.* ***g-i)*** *Displays the correlation between the frequency (in cps) at which the maximum fit was reached and stride-cycle duration. All correlations are non-significant after correction for multiple comparisons.*

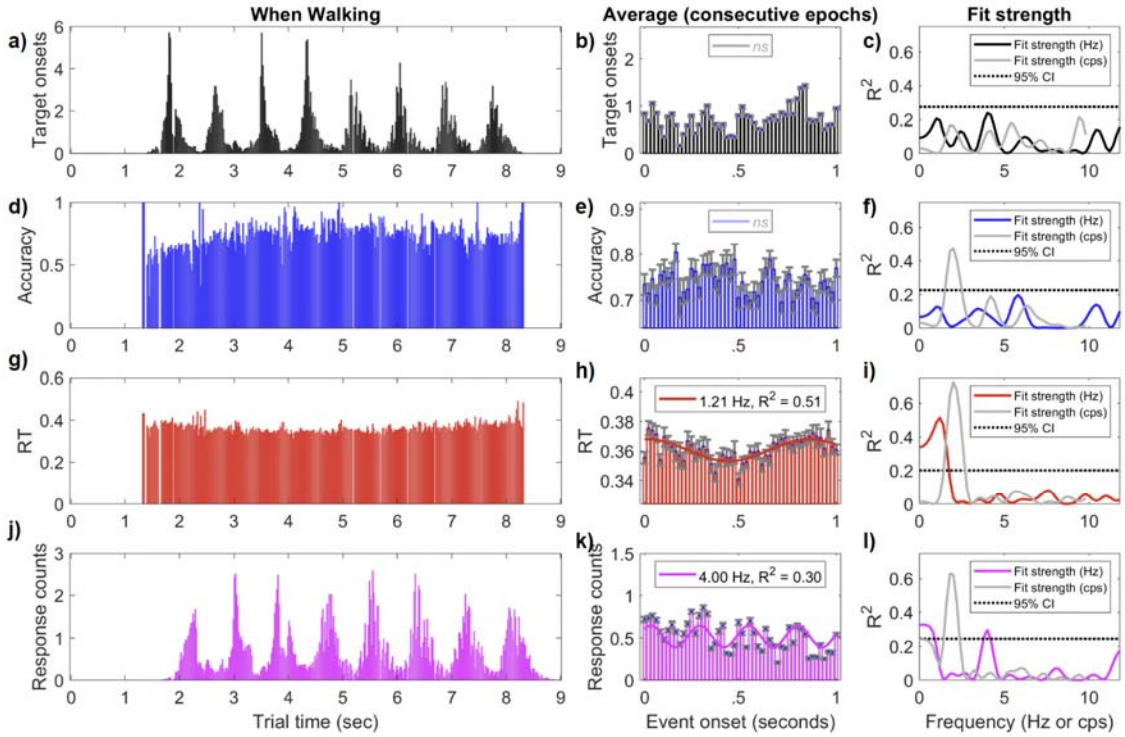

Supplementary Figure 6*. An analysis of perceptual oscillations when walking, aligned to clock-time.* ***a)*** *plots the distribution of all target onsets within each 9 second trial, averaged across participants. The oscillatory structure in target onsets is expected based on our jittered-target spacing. Critically, we note that despite this structure, the presentation of target onsets within a stride was approximately uniform (cf. Manuscript Figure 3C), owing to the variability of stride times across participants.* ***b)*** *Displays the average over all consecutive 1 second epochs (20 ms bins, no overlap). No oscillations were present above the 95% CI of shuffled data.* ***c)*** *displays the goodness-of-fit for all frequencies in Hz in black. Overlaid in grey is the equivalent strength of Fourier fits using the cycles-per-stride data (i.e. Manuscript Figure 3). Broken lines display the 95% CI for data aligned to clock-time****. d)*** *Displays the change in target accuracy over trial-time, while walking.* ***e)*** *displays the change in accuracy on average over 1 second epochs.* ***f)*** *Demonstrates that the strength of accuracy oscillations per stride-cycle (grey) far exceeds the strength of any oscillation per second (blue).* ***g,h,i)*** *The same data for reaction times in red. Again note that the fit-strength when aligning to cycles-per-stride far exceeds oscillations in Hz.* ***j,k,l)*** *Displays the response counts per trial time, per second, and fit strength, respectively. Although there is temporal structure owing to our target spacing, fit strength during cycles-per-stride far exceeds fit-strength in units of time, demonstrating that perceptual oscillations are locked to the phase of the stride-cycle.*

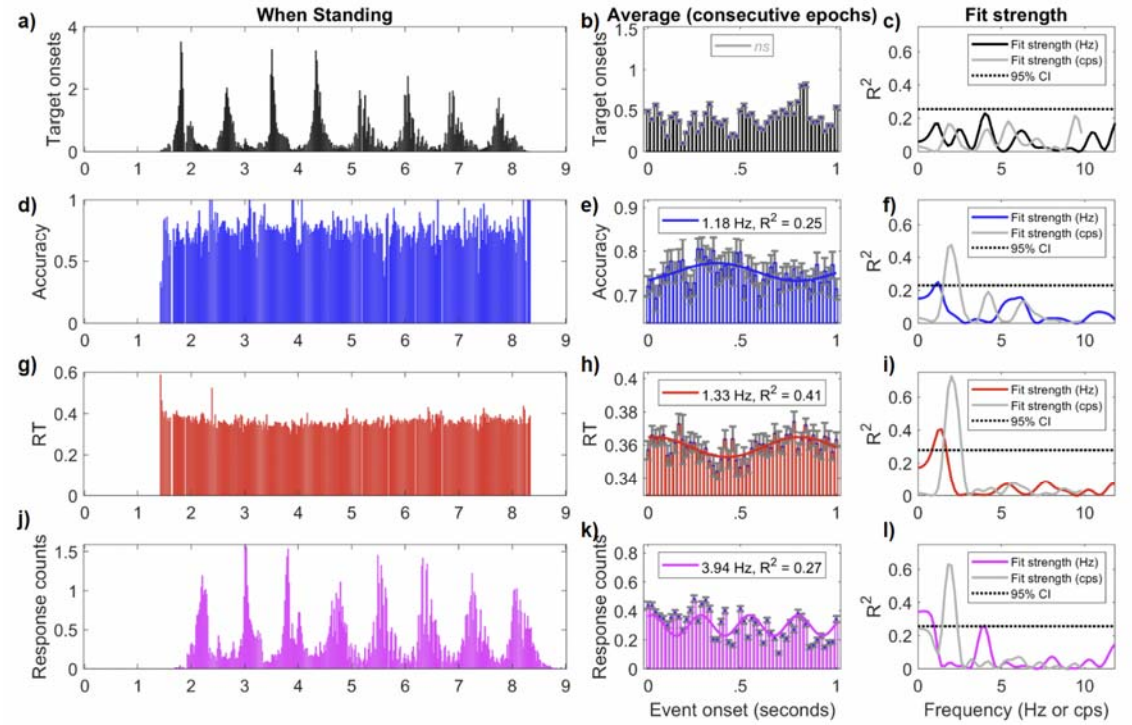

Supplementary Figure 7*. An analysis of perceptual oscillations when stationary, aligned to clock-time.* ***a)*** *plots the distribution of all target onsets within each 9 second trial, averaged across participants. The oscillatory structure in target onsets is expected based on our jittered-target spacing. Critically, we note that despite this structure, the presentation of target onsets within a stride was approximately uniform (cf. Manuscript Figure 3C), owing to the variability of stride times across participants.* ***b)*** *Displays the average over all consecutive 1 second epochs (20 ms bins, no overlap). No oscillations were present above the 95% CI of shuffled data.* ***c)*** *displays the goodness-of-fit for all frequencies in Hz in black. Overlaid in grey is the equivalent strength of Fourier fits using the cycles-per-stride data (i.e. Manuscript Figure 3). Broken lines display the 95% CI for data aligned to clock-time.* ***d)*** *Displays the change in target accuracy over trial-time, while walking.* ***e)*** *displays the change in accuracy on average over 1 second epochs.* ***f)*** *Demonstrates that the strength of accuracy oscillations per stride-cycle (grey) far exceeds the strength of any oscillation per second (blue****). g,h,i)*** *The same data for reaction times in red. Again note that the fit-strength when aligning to cycles-per-stride far exceeds oscillations in Hz.****j,k,l****) Displays the response counts per trial time, per second, and fit strength, respectively. Although there is temporal structure owing to our target spacing, fit strength during cycles-per-stride far exceeds fit-strength in units of time, demonstrating that perceptual oscillations are locked to the phase of the stride-cycle.*

References

Allen, M., Varga, S., & Heck, D. H. (2022). Respiratory rhythms of the predictive mind. *Psychological Review*. https://doi.org/10.1037/rev0000391

Al-Yahya, E., Dawes, H., Smith, L., Dennis, A., Howells, K., & Cockburn, J. (2011). Cognitive motor interference while walking: a systematic review and meta-analysis. *Neuroscience and Biobehavioral Reviews*, *35*(3), 715–728.

Ayaz, A., Saleem, A. B., Schölvinck, M. L., & Carandini, M. (2013). Locomotion controls spatial integration in mouse visual cortex. *Current Biology: CB*, *23*(10), 890–894.

Azzalini, D., Rebollo, I., & Tallon-Baudry, C. (2019). Visceral Signals Shape Brain Dynamics and Cognition. *Trends in Cognitive Sciences*, *23*(6), 488–509.

Benedetto, A., Spinelli, D., & Morrone, M. C. (2016). Rhythmic modulation of visual contrast discrimination triggered by action. *Proceedings. Biological Sciences / The Royal Society*, *283*(1831), 20160692.

Bent, L. R., Inglis, J. T., & McFadyen, B. J. (2004). When is vestibular information important during walking? *Journal of Neurophysiology*, *92*(3), 1269–1275.

Berens, P. (2009). CircStat: A MATLAB Toolbox for Circular Statistics. *Journal of Statistical Software*, *31*, 1–21.

Bernasconi, P., & Kohl, J. (1993). Analysis of co-ordination between breathing and exercise rhythms in man. *The Journal of Physiology*, *471*(1), 693–706.

Bramble, D. M., & Carrier, D. R. (1983). Running and breathing in mammals. *Science*, *219*(4582), 251–256.

Bullock, T., Elliott, J. C., Serences, J. T., & Giesbrecht, B. (2017). Acute Exercise Modulates Feature-selective Responses in Human Cortex. *Journal of Cognitive Neuroscience*, *29*(4), 605–618.

Burkitt, J. J., Campos, J. L., & Lyons, J. L. (2020). Iterative Spatial Updating During Forward Linear Walking Revealed Using a Continuous Pointing Task. *Journal of Motor Behavior*, *52*(2), 145–166.

Busse, L., Cardin, J. A., Chiappe, M. E., Halassa, M. M., McGinley, M. J., Yamashita, T., & Saleem, A. B. (2017). Sensation during Active Behaviors. *The Journal of Neuroscience: The Official Journal of the Society for Neuroscience*, *37*(45), 10826–10834.

Cao, L., Chen, X., & Haendel, B. F. (2020). Overground walking decreases alpha activity and entrains eye movements in humans. *Frontiers in Human Neuroscience*, *14*, 561755.

Cao, L., & Händel, B. (2019). Walking enhances peripheral visual processing in humans. *PLoS Biology*, *17*(10), e3000511.

Carpenter, R. (1988). *Movements of the eyes*. *2*, 593.

Carpenter, R. (2000). The neural control of looking. *Current Biology: CB*, *10*(8), R291–R293.

Chang, Y. K., Labban, J. D., Gapin, J. I., & Etnier, J. L. (2012). The effects of acute exercise on cognitive performance: a meta-analysis. *Brain Research*, *1453*, 87–101.

Chen, X., Cao, L., & Haendel, B. (2022a). Differential effects of walking across visual cortical processing stages. *Cortex; a Journal Devoted to the Study of the Nervous System and Behavior*. https://doi.org/10.1016/j.cortex.2022.01.007

Chen, X., Cao, L., & Haendel, B. F. (2022b). Human visual processing during walking: Dissociable pre- and post-stimulus influences. *NeuroImage*, *264*, 119757.

Chiovetto, E., & Giese, M. A. (2013). Kinematics of the coordination of pointing during locomotion. *PloS One*, *8*(11), e79555.

Cortney Bradford, J., Lukos, J. R., Passaro, A., Ries, A., & Ferris, D. P. (2019). Effect of locomotor demands on cognitive processing. *Scientific Reports*, *9*(1), 9234.

Cousineau, D. (2005). Confidence intervals in within-subject designs: A simpler solution to Loftus and Masson's method. *Tutorials in Quantitative Methods for Psychology*, *1*(1), 42–45.

Critchley, H. D., & Harrison, N. A. (2013). Visceral influences on brain and behavior. *Neuron*, *77*(4), 624–638.

Dakin, C. J., Inglis, J. T., Chua, R., & Blouin, J.-S. (2013). Muscle-specific modulation of vestibular reflexes with increased locomotor velocity and cadence. *Journal of Neurophysiology*, *110*(1), 86–94.

Davidson, M. J., Alais, D., van Boxtel, J. J. A., & Tsuchiya, N. (2018). Attention periodically samples competing stimuli during binocular rivalry. *eLife*, *7*, e40868.

Davidson, M. J., Keys, R. T., Szekely, B., MacNeilage, P., Verstraten, F., & Alais, D. (2023). Peripersonal tracking accuracy is limited by the speed and phase of locomotion. In *bioRxiv* (p. 2023.04.17.537137). https://doi.org/10.1101/2023.04.17.537137

Dickinson, M. H., Farley, C. T., Full, R. J., Koehl, M. A., Kram, R., & Lehman, S. (2000). How animals move: an integrative view. *Science*, *288*(5463), 100–106.

Dipoppa, M., Ranson, A., Krumin, M., Pachitariu, M., Carandini, M., & Harris, K. D. (2018). Vision and Locomotion Shape the Interactions between Neuron Types in Mouse Visual Cortex. *Neuron*, *98*(3), 602–615.e8.

Dodwell, G., Liesefeld, H. R., Conci, M., Müller, H. J., & Töllner, T. (2021). EEG evidence for enhanced attentional performance during moderate-intensity exercise. *Psychophysiology*, e13923.

Drew, T., & Marigold, D. S. (2015). Taking the next step: cortical contributions to the control of locomotion. *Current Opinion in Neurobiology*, *33*, 25–33.

Fiebelkorn, I. C., & Kastner, S. (2019). A rhythmic theory of attention. *Trends in Cognitive Sciences*, *23*(2), 87–101.

Fiebelkorn, I. C., Pinsk, M. A., & Kastner, S. (2018). A Dynamic Interplay within the Frontoparietal Network Underlies Rhythmic Spatial Attention. *Neuron*, *99*(4), 842–853.e8.

Gard, S. A., Miff, S. C., & Kuo, A. D. (2004). Comparison of kinematic and kinetic methods for computing the vertical motion of the body center of mass during walking. *Human Movement Science*, *22*(6), 597–610.

Garrett, J., Bullock, T., & Giesbrecht, B. (2021). Tracking the Contents of Spatial Working Memory during an Acute Bout of Aerobic Exercise. *Journal of Cognitive Neuroscience*, *33*(7), 1271–1286.

Grillner, S., & El Manira, A. (2020). Current Principles of Motor Control, with Special Reference to Vertebrate Locomotion. *Physiological Reviews*, *100*(1), 271–320.

Harrower, M., & Brewer, C. A. (2003). ColorBrewer.org: An Online Tool for Selecting Colour Schemes for Maps. *The Cartographic Journal*, *40*(1), 27–37.

Heck, D. H., McAfee, S. S., Liu, Y., Babajani-Feremi, A., Rezaie, R., Freeman, W. J., Wheless, J. W., Papanicolaou, A. C., Ruszinkó, M., & Kozma, R. (2016). Cortical rhythms are modulated by respiration. In *bioRxiv* (p. 049007). https://doi.org/10.1101/049007

Heck, D. H., McAfee, S. S., Liu, Y., Babajani-Feremi, A., Rezaie, R., Freeman, W. J., Wheless, J. W., Papanicolaou, A. C., Ruszinkó, M., Sokolov, Y., & Kozma, R. (2016). Breathing as a Fundamental Rhythm of Brain Function. *Frontiers in Neural Circuits*, *10*, 115.

Hillnhütter, H. (2022). Stimulating urban walking environments – Can we measure the effect? *Environment and Planning B: Urban Analytics and City Science*, *49*(1), 275–289.

Hirasaki, E., Moore, S. T., Raphan, T., & Cohen, B. (1999). Effects of walking velocity on vertical head and body movements during locomotion. *Experimental Brain Research. Experimentelle Hirnforschung. Experimentation Cerebrale*, *127*(2), 117–130.

Ho, H. T., Leung, J., Burr, D. C., Alais, D., & Morrone, M. C. (2017). Auditory sensitivity and decision criteria oscillate at different frequencies separately for the two ears. *Current Biology: CB*, *27*(23), 3643–3649.e3.

Ince, R. A., Kay, J. W., & Schyns, P. G. (2022). Within-participant statistics for cognitive science. *Trends in Cognitive Sciences*, *0*(0). https://doi.org/10.1016/j.tics.2022.05.008

Ince, R. A., Paton, A. T., Kay, J. W., & Schyns, P. G. (2021). Bayesian inference of population prevalence. *eLife*, *10*. https://doi.org/10.7554/eLife.62461

Keller, G. B., Bonhoeffer, T., & Hübener, M. (2012). Sensorimotor mismatch signals in primary visual cortex of the behaving mouse. *Neuron*, *74*(5), 809–815.

Kirby, R. L., Nugent, S. T., Marlow, R. W., MacLeod, D. A., & Marble, A. E. (1989). Coupling of cardiac and locomotor rhythms. *Journal of Applied Physiology*, *66*(1), 323–329.

Klimesch, W. (2018). The frequency architecture of brain and brain body oscillations: an analysis. *The European Journal of Neuroscience*, *48*(7), 2431–2453.

Kluger, D. S., Balestrieri, E., Busch, N. A., & Gross, J. (2021). Respiration aligns perception with neural excitability. *eLife*, *10*. https://doi.org/10.7554/eLife.70907

Kluger, D. S., & Gross, J. (2021). Respiration modulates oscillatory neural network activity at rest. *PLoS Biology*, *19*(11), e3001457.

Lacquaniti, F., Grasso, R., & Zago, M. (1999). Motor Patterns in Walking. *News in Physiological Sciences: An International Journal of Physiology Produced Jointly by the International Union of Physiological Sciences and the American Physiological Society*, *14*, 168–174.

Landau, A. N., & Fries, P. (2012). Attention samples stimuli rhythmically. *Current Biology: CB*, *22*(11), 1000–1004.

Lee, H.-T., & Banzett, R. B. (1997). Mechanical Links Between Locomotion and Breathing: Can You Breathe With Your Legs? *Physiology* , *12*(6), 273–278.

Lunghi, C., & Sale, A. (2015). A cycling lane for brain rewiring. *Current Biology: CB*, *25*(23), R1122–R1123.

MacNeilage, P. R. (2020). Characterization of Natural Head Movements in Animals and Humans. In Fritzsch Bernd & Straka (Ed.), *The Senses: A Comprehensive Reference (Second Edition)* (Vol. 392, pp. 69–87). Elsevier.

MacNeilage, P. R., & Glasauer, S. (2017). Quantification of Head Movement Predictability and Implications for Suppression of Vestibular Input during Locomotion. *Frontiers in Computational Neuroscience*, *11*. https://doi.org/10.3389/fncom.2017.00047

Matthis, J. S., Barton, S. L., & Fajen, B. R. (2017). The critical phase for visual control of human walking over complex terrain. *Proceedings of the National Academy of Sciences of the United States of America*, *114*(32), E6720–E6729.

Matthis, J. S., & Fajen, B. R. (2013). Humans exploit the biomechanics of bipedal gait during visually guided walking over complex terrain. *Proceedings. Biological Sciences / The Royal Society*, *280*(1762), 20130700.

Matthis, J. S., Yates, J. L., & Hayhoe, M. M. (2018). Gaze and the Control of Foot Placement When Walking in Natural Terrain. *Current Biology: CB*, *28*(8), 1224–1233.e5.

Moore, S. T., Hirasaki, E., Raphan, T., & Cohen, B. (2001). The human vestibulo-ocular reflex during linear locomotion. *Annals of the New York Academy of Sciences*, *942*, 139–147.

Mulavara, A. P., & Bloomberg, J. J. (2002). Identifying head-trunk and lower limb contributions to gaze stabilization during locomotion. *Journal of Vestibular Research: Equilibrium & Orientation*, *12*(5-6), 255–269.

Niell, C. M., & Stryker, M. P. (2010). Modulation of visual responses by behavioral state in mouse visual cortex. *Neuron*, *65*(4), 472–479.

Niizeki, K., Kawahara, K., & Miyamoto, Y. (1993). Interaction among cardiac, respiratory, and locomotor rhythms during cardiolocomotor synchronization. *Journal of Applied Physiology*, *75*(4), 1815–1821.

Niizeki, K., Kawahara, K., & Miyamoto, Y. (1996). Cardiac, respiratory, and locomotor coordination during walking in humans. *Folia Primatologica; International Journal of Primatology*, *66*(1-4), 226–239.

Niizeki, K., & Saitoh, T. (2014). Cardiolocomotor phase synchronization during rhythmic exercise. *The Journal of Physical Fitness and Sports Medicine*, *3*(1), 11–20.

Parker, P. R. L., Brown, M. A., Smear, M. C., & Niell, C. M. (2020). Movement-Related Signals in Sensory Areas: Roles in Natural Behavior. *Trends in Neurosciences*, *43*(8), 581–595.

Park, H.-D., Correia, S., Ducorps, A., & Tallon-Baudry, C. (2014). Spontaneous fluctuations in neural responses to heartbeats predict visual detection. *Nature Neuroscience*, *17*(4), 612–618.

Polack, P.-O., Friedman, J., & Golshani, P. (2013). Cellular mechanisms of brain state-dependent gain modulation in visual cortex. *Nature Neuroscience*, *16*(9), 1331–1339.

Pozzo, T., Berthoz, A., & Lefort, L. (1990). Head stabilization during various locomotor tasks in humans. I. Normal subjects. *Experimental Brain Research. Experimentelle Hirnforschung. Experimentation Cerebrale*, *82*(1), 97–106.

Romei, V., Gross, J., & Thut, G. (2012). Sounds reset rhythms of visual cortex and

corresponding human visual perception. *Current Biology: CB*, *22*(9), 807–813.

Saleem, A. B., Ayaz, A., Jeffery, K. J., Harris, K. D., & Carandini, M. (2013). Integration of visual motion and locomotion in mouse visual cortex. *Nature Neuroscience*, *16*(12), 1864–1869.

Schütt, H. H., Harmeling, S., Macke, J. H., & Wichmann, F. A. (2016). Painfree and accurate Bayesian estimation of psychometric functions for (potentially) overdispersed data. *Vision Research*, *122*, 105–123.

Tomassini, A., Ambrogioni, L., Medendorp, W. P., & Maris, E. (2017). Theta oscillations locked to intended actions rhythmically modulate perception. *eLife*, *6*(e25618). https://doi.org/10.7554/eLife.25618

Tomassini, A., Spinelli, D., Jacono, M., Sandini, G., & Morrone, M. C. (2015). Rhythmic oscillations of visual contrast sensitivity synchronized with action. *The Journal of Neuroscience: The Official Journal of the Society for Neuroscience*, *35*(18), 7019–7029.

Tosato, T., Rohenkohl, G., Dowdall, J. R., & Fries, P. (2022). Quantifying rhythmicity in perceptual reports. *NeuroImage*, *262*, 119561.

VanRullen, R. (2015). Perceptual cycles. *Trends in Cognitive Sciences*, *15*(12), 723–735.

VanRullen, R. (2016). Perceptual Rhythms. *Stevens' Handbook of Experimental Psychology*, 1–51.

VanRullen, R. (2018). Attention Cycles. *Neuron*, *99*(4), 632–634.

VanRullen, R., Carlson, T., & Cavanagh, P. (2007). The blinking spotlight of attention. *Proceedings of the National Academy of Sciences of the United States of America*, *104*(49), 19204–19209.

Varga, S., & Heck, D. H. (2017). Rhythms of the body, rhythms of the brain: Respiration, neural oscillations, and embodied cognition. *Consciousness and Cognition*, *56*, 77–90.

Watson, A. B., & Pelli, D. G. (1983). QUEST: a Bayesian adaptive psychometric method. *Perception & Psychophysics*, *33*(2), 113–120.

Wutz, A., Muschter, E., van Koningsbruggen, M. G., Weisz, N., & Melcher, D. (2016). Temporal integration windows in neural processing and perception aligned to saccadic

eye movements. *Current Biology: CB*, *26*(13), 1659–1668.

Zhang, H., Morrone, M. C., & Alais, D. (2019). Behavioural oscillations in visual orientation discrimination reveal distinct modulation rates for both sensitivity and response bias. *Scientific Reports*, *9*(1), 1115.